HHS Public Access

Author manuscript

J Mol Med (Berl). Author manuscript; available in PMC 2017 September 01.

Published in final edited form as:

J Mol Med (Berl). 2016 September ; 94(9): 1053–1062. doi:10.1007/s00109-016-1410-7.

The R130S mutation significantly affects the function of prestin, the outer hair cell motor protein

Satoe Takahashi[1], **Mary Ann Cheatham**[2,3], **Jing Zheng**[1,2], and **Kazuaki Homma**[1,2,*]

[1]Department of Otolaryngology – Head and Neck Surgery, Feinberg School of Medicine, Northwestern University, Chicago, IL 60611, USA

[2]The Hugh Knowles Center for Clinical and Basic Science in Hearing and Its Disorders, Northwestern University, Evanston, IL 60208, USA

[3]Department of Communication Sciences and Disorders, Northwestern University, Evanston, IL 60208, USA

Abstract

A missense mutation, R130S, was recently found in the prestin gene, *SLC26A5*, of patients with moderate to severe hearing loss (DFNB61). In order to define the pathology of hearing loss associated with this missense mutation, a recombinant prestin construct harboring the R130S mutation (R130S-prestin) was generated, and its functional consequences examined in a heterologous expression system. We found that R130S-prestin targets the plasma membrane but less efficiently compared to wild-type. The voltage operating point and voltage sensitivity of the motor function of R130S-prestin were similar to wild-type prestin. However, the motor activity of R130S-prestin is greatly reduced at higher voltage stimulus frequencies, indicating a reduction in motor kinetics. Our study thus provides experimental evidence that supports a causal relationship between the R130S mutation in the prestin gene and hearing loss found in patients with this missense mutation.

Keywords

DFNB61; prestin; SLC26A5; hearing loss; electromotility; anion transport

INTRODUCTION

SLC26 constitutes a large and functionally diverse protein family. SLC26 proteins work as anion exchangers, but some members can also work as anion channels (SLC26A7, SLC26A9, SLC26A11) or even as a voltage-operated motor (SLC26A5) [1]. Mutations in SLC26 proteins are associated with various human diseases such as nephrocalcinosis (SLC26A1), diastrophic dysplasia (SLC26A2), achondrogenesis (SLC26A2), atelosteogenesis (SLC26A2), multiple epiphyseal dysplasia (SLC26A2), congenital chloride

*Address correspondence to: Kazuaki Homma, 303 E Chicago Ave, Chicago, IL 60611. Tel: 312-503-5344, FAX: 312-503-1616, k-homma@northwestern.edu.

CONFLICT OF INTEREST

The authors declare that there is no conflict of interest.

diarrhea (SLC26A3), Pendred syndrome (SLC26A4), hearing loss/deafness (SLC26A4 and SLC26A5), asthenozoospermia (SLC26A8), and bronchiectasis (SLC26A9) [1].

Prestin (SLC26A5) is the membrane protein that confers voltage-dependent mechanical activity, often referred to as somatic electromotility, on auditory outer hair cells (OHCs) [2]. OHC electromotility is presumed to minimize the effect of viscous damping by the cochlear fluids in a cycle-by-cycle manner at audible frequencies, thereby supporting the high sensitivity and frequency selectivity of mammalian ears. The essential requirements of prestin and its voltage-operated motor activity for normal cochlear operation have been demonstrated using several prestin mouse models [3–7]. However, pathogenicity of prestin mutation in human patients has been ambiguous. A previous study found the IVS2-2A>G variation in the SLC26A5 gene is associated with hearing loss [8]. This single A-to-G nucleotide conversion is presumed to compromise the production of prestin protein by disrupting the proper splicing of the third exon of *SLC26A5*, which contains the start codon (OMIM 613865). However, later studies question the pathogenicity of this variation [9, 10].

Recently, two young Japanese siblings (6 and 9 years old) with moderate to severe hearing loss were found to have compound heterozygous *SLC26A5* c.209G >A (p.W70X) and c. 390A >C (p.R130S) mutations [11]. Their parents were found to have heterozygous *SLC26A5* mutations with either p.W70X or p.R130S, but without hearing impairment [11]. Examining the functional consequences of these mutations is essential for demonstrating the pathogenicity of these mutations and for defining the disease mechanism. It is likely that the premature translation termination caused by the W70X nonsense mutation induces nonsense-mediated mRNA decay [12]. The N-terminal cytosolic domain of prestin is comprised of the first ~80 amino acids, and does not contain any transmembrane domain [13]. Therefore, prestin with W70X would not target the cell membrane even if it were translated. Thus, it is conceivable that the functional consequence of the W70X mutation is a functional null [3–6]. In this study, we focus on the R130S mutation, and demonstrate that this missense mutation significantly affects membrane targeting, voltage-dependent motility, and anion transport function of prestin.

MATERIALS AND METHODS

Generation of a structural model of prestin

The structural model of the transmembrane region of prestin shown in Fig. 1 was generated by Phyre2 [14] based on the SLC26Dg structure (5DA0) [15] using the partial amino acid sequence (P72 – R502) of human prestin (P58743).

Generation of an R130S-prestin construct and transfection of HEK293T cells

The R130S missense mutation was introduced to gerbil prestin cloned into a pECFP-N2 vector using a pair of mutagenic DNA primers (5′-GGACCTCCAGTCACATATCTATAGGTCCTTTC-3′ and 5′-GATATGTGACTGGAGGTCCCAAAGAAACAG-3′). Transfection of HEK293T cells was performed as described previously [16]. Transfected cells were used for experiments (imaging and electrophysiology) between 48 and 72 hrs post transfection.

Bioinformatics

Five hundred non-redundant protein sequences were obtained by PSI-BLAST search using the human prestin amino acid sequence (P58743) as a query. The BLAST search was repeated until no new sequence was obtained (total ten iterations). The obtained sequences were aligned using Clustal Omega (http://www.clustal.org/omega/) in order to generate sequence logos using WebLogo [17] (Fig. 2b).

Cell imaging

HEK293T cells were grown on a cover glass in 24-well plates and were transfected with wt- or R130S-prestin-ECFP plasmids using Effectene Transfection Reagent (QIAGEN) according to the manufacturer's instruction manual. At 48–72 hrs post transfection, the cells were fixed with 4% formaldehyde for 5 min at room temperature, stained with 5 μM DiI, a lipophilic dye retained in the plasma membrane (Molecular Probes, D282) and 1 μg/ml Hoechst 33342, a nucleic acid dye to facilitate cell identification (Molecular Probes, H3570) for 10 min at room temperature before mounting onto slides using Dako fluorescent mounting medium (DAKO). Images were captured using the Nikon A1R confocal microscope with Plan Apo 60X oil objective (Nikon), and analyzed using NIS-Elements software (Nikon) to generate intensity profile plots on Prism (GraphPad).

Biotinylation of membrane-targeted prestin and its quantification

HEK293T cells ($1.6–2.0 \times 10^6$) were grown in a 10-cm culture dish and were transfected with wt- or R130S-prestin-ECFP plasmids using Effectene Transfection Reagent (QIAGEN) according to the manufacturer's instructions. ECFP-expressing plasmids were used as negative controls. At 48–72 hrs post transfection, the cell surface proteins were biotinylated using a Cell Surface Protein Isolation Kit (Thermo Scientific). Biotinylated prestins were isolated according to the manufacturer's manual except that lysis, wash, and elution buffers contained (mM): 154 NaCl, 1 EGTA, 20 n-Dodecyl-β-D-maltoside, and 10 Tris-Cl (pH 7.4). ECFP fluorescence was measured using Synergy 2 Multi-Mode Microplate Reader (BioTek).

Cell membrane electric capacitance measurement

The electric current response to a sinusoidal voltage stimulus (1-Hz, 120 mV amplitude), superimposed with two higher frequency stimuli (390.6 (f_1) and 781.2 (f_2) Hz, 10 mV amplitude), was recorded in the whole-cell configuration at room temperature using the Axopatch 200A amplifier (Molecular Devices, Sunnyvale, CA). Cell membrane electric capacitance was determined by a fast Fourier transform-based admittance analysis [18] using jClamp (SciSoft Company, New Haven, CT). Recording pipettes were pulled from borosilicate glass to achieve initial bath resistances averaging 3–4 MΩ. An intracellular solution contained (mM): 140 CsCl, 2 $MgCl_2$, 10 EGTA, and 10 HEPES (pH 7.4). An extracellular (bath) solution contained (mM): 120 NaCl, 20 TEA-Cl, 2 $CoCl_2$, 2 $MgCl_2$, 10 HEPES (pH 7.4). Osmolarity was adjusted to 320 mmol/kg with glucose. Intracellular pressure was kept at 0 mmHg. For stimulus frequency-dependent capacitance measurements, f_1 was set at 195.3 (f_2=390.6), 390.6 (f_2=781.3), 781.3 (f_2=1562.5), 1562.5 (f_2=3125.0), and 3125.0 (f_2=6250.0) Hz [19].

Nonlinear capacitance data analysis

Voltage-dependent cell membrane electric capacitance data were analyzed using the following two-state Boltzmann equation:

$$C_m = \frac{\alpha Q_{\max} \exp[\alpha(V_m - V_{pk})]}{\{1+\exp[\alpha(V_m - V_{pk})]\}^2} + C_{lin}$$

where α is the slope factor of the voltage-dependence of charge transfer, Q_{max} is the maximum charge transfer, V_m is the membrane potential, V_{pk} is the voltage at which the maximum charge movement is attained, and C_{lin} is the linear capacitance [16, 19–21].

Anion transport assay

Anion transport activity of prestin was determined electrophysiologically in the whole-cell configuration at room temperature using the Axopatch 200A amplifier (Molecular Devices, Sunnyvale, CA). Similar recording pipettes used for capacitance measurements (see above) were filled with an intracellular solution contained (mM): 150 CsCl, 2 $MgCl_2$, 10 EGTA, and 10 HEPES (pH 7.4). Cells were bathed in an extracellular solution contained (mM): 150 NaCl, 2 $CoCl_2$, 2 $MgCl_2$, 10 HEPES (pH 7.4, 324 mmol/kg). Perfusate contained (mM): 150 NaSCN, 2 $CoCl_2$, 2 $MgCl_2$, 10 HEPES (pH 7.4, 330 mmol/kg). A sinusoidal voltage stimulus (1-Hz, 120 mV amplitude), superimposed with two higher frequency stimuli (390.6 and 781.2 Hz, 10 mV amplitude), was used for determining NLC.

Statistical analysis

Curve fits and statistical analyses were performed using Prism (GraphPad software) except for the F-test (see below). The Student's t-test was used for comparisons between two groups. A one-sample t-test was performed for data that were corrected for matched normalized control (wild-type) data in Fig. 3c. One-way analysis of variance combined with the Tukey test was used for multiple comparisons. The F-test was performed using the FDIST function in Excel (Microsoft) with parameters obtained from linear regressions. $p < 0.05$ was considered statistically significant.

RESULTS

The R130 site

The structure of prestin has not been solved except for a portion of the C-terminal cytosolic domain [22]. However, Gorbunov and colleagues proposed structural models for prestin [13] based on bioinformatic and biochemical analyses. The veracity of these prestin models is strongly supported by the structure recently determined for bacterial SLC26 protein, SLC26Dg [15]. Figure 1 shows a structural model of prestin generated by Phyre2 [14] based on the structure of SLC26Dg. The R130 site is located at the C-terminal end of the SulP motif (Prosite PS01130) (Fig. 1), a region highly conserved among members of the SLC26/SulP transporter family (Fig. 2). Many disease-associated missense mutations have also been found in this region of SLC26 proteins (highlighted in gray in Fig. 2a) [11, 23–34], implying

general importance of this region for the basic architecture and/or function shared among the SLC26/SulP proteins.

Effect of the R130S mutation on membrane targeting of prestin protein

In order to assess how the function of prestin could be affected by the R130S mutation, a recombinant R130S-prestin (full-length) with an ECFP tag at the C-terminus (R130S-prestin-ECFP) was generated, and heterologously expressed in HEK293T cells. The ECFP fluorescence not only facilitated identification of cells expressing R130S-prestin during whole-cell recording experiments (see below), but it also allowed assessment of the subcellular localization of expressed protein. Figure 3 shows examples of HEK293T cells expressing either wild-type (wt)-prestin-ECFP (two examples in Fig. 3a) or R130S-prestin-ECFP (two examples in Fig. 3b). The cells were stained with DiI in order to label the plasma membrane. For wt, the peaks for the DiI (dashed lines) and the ECFP fluorescence (solid lines) align as indicated by the downward pointing arrows in Fig. 3a. In contrast, the localization of the ECFP signal at the plasma membrane was usually ambiguous in cells expressing R130S-prestin-ECFP compared to those expressing wt-prestin-ECFP although the ECFP signal was evident in the cytosolic compartments of most cells.

In a separate experiment, we biotinylated cell surface proteins, and quantified the amount of affinity isolated prestin proteins at the cell surface by measuring ECFP fluorescence (see Materials and Methods). ECFP fluorescence intensity determined for wt-prestin-ECFP was normalized to unity and relative fluorescence intensities determined for R130-prestin-ECFP and ECFP alone (the negative control for cell surface protein biotinylation) for each experiment. As expected, very low ECFP fluorescence was detected for ECFP control (Fig. 3c), affirming that biotinylation is minimal for proteins not targeted to the cell membrane. In all experimental repeats (n=4), ECFP fluorescence was smaller for R130S-prestin-ECFP compared to wt-prestin-ECFP (66% on average, Fig. 3c). A one-sample t-test found that this difference was statistically significant ($p=0.0069$). Consistent with the bright ECFP signals found in the cytosols of both wt- and R130S-prestin-expressing cells (Fig. 3a and 3b), strong ECFP fluorescence was detected in the flow-through (non-biotinylated fraction) for both wt- and R130S-prestin without statistically significant difference ($p=0.51$).

Collectively, these observations suggest that the R130S mutation impairs membrane targeting, consistent with previous studies suggesting the importance of the R130 region within the prestin molecule for targeting [13, 35].

Effect of the R130S mutation on the motor function of prestin

In order to assess the effect of the R130S mutation on prestin's motor function, we recorded whole-cell nonlinear capacitance (NLC) in HEK293T cells expressing R130S-prestin-ECFP, and compared the results to those recorded using wt-prestin-ECFP-expressing cells (Fig. 4). NLC data are commonly used for evaluating the motor activities of prestin and its mutants since NLC provides an electrical signature of the voltage-operated motor function of prestin [36, 37]. Targeting of prestin protein to the cell membrane is a prerequisite for a successful NLC recording, and the magnitude of NLC correlates with the amount of prestin expressed

in the cell membrane. Therefore, NLC measurements also provide unequivocal quantitative evidence regarding membrane targeting.

Heterologous expression of R130S-prestin-ECFP conferred NLC on HEK293T cells (Fig. 4a). The voltage sensitivity (α, Fig. 4b) and the peak voltage operating point (V_{pk}, Fig. 4c) of R130S-prestin were comparable to those of wt-prestin, indicating that R130S-prestin is functional as a voltage-operated motor. The magnitudes of the NLC obtained from R130S-prestin-expressing cells, however, were much smaller compared to those obtained from wt-prestin-expressing cells (Fig. 4a). Since larger cells tend to harbor greater amounts of prestin protein in the cell membrane, we divided Q_{max}, which is represented by the area under an NLC curve and correlates with the total amount of prestin, by C_{lin}, which is voltage-independent and correlates with the surface area of a cell. The resulting quotient (Q_{max}/C_{lin}), referred to as charge density, was used for comparing the amount of functional prestin expressed on the surface of cells for R130S- vs. wt-prestin. As shown in Fig. 4d, the charge densities of R130S-prestin-expressing cells were significantly smaller than those of wt-prestin-expressing cells, suggesting that the R130S mutation impairs membrane targeting of prestin. We also noticed that many R130S-prestin-expressing cells (~50%) did not show detectable NLC although they were clearly ECFP-positive. These observations are consistent with the visual assessment of membrane targeting made by ECFP fluorescence imaging (Fig. 3), i.e., the predominately cytoplasmic expression of mutated R130S prestin protein. However, the smaller charge density of R130S-prestin-expressing cells (~6 fC/pF) compared to wt-prestin-expressing cells (~18 fC/pF) cannot be explained solely by the reduced amount of membrane-targeted R130S-prestin (~66%, Fig. 3c). This observation suggests that the R130S mutation also impairs the motor function of prestin (see below).

OHC electromotility supported by the voltage-operated motor function of prestin is presumed to work against fluid friction in the cochlea at audible frequencies in humans (20–20,000 Hz). Thus, any mutation that impairs the fast motor kinetics of prestin should reduce OHC electromotility, and could compromise hearing. In order to test if the R130S mutation has such an effect, we measured NLC in a stimulus frequency-dependent manner [19, 38, 39]. Cell membrane electric capacitance (C_m) recording is based on the measurement of capacitive charge movement. Prestin-associated charge movement, a signature of its motor function, is also detected as C_m (NLC) since it is as fast as capacitive charge movement. Therefore, if stimulus frequency exceeded the motor kinetics of prestin, an underestimation of prestin-associated charge movement, i.e., Q_{max}, would manifest as a reduction of NLC. In the typical whole-cell recording configuration, the stimulus voltage frequencies used for measuring C_m are determined by the series resistance (R_s) and the cell membrane resistance (R_m) because these resistances limit the overall circuit admittance at high and low frequency regions where measured admittance no longer correlates with the magnitude of C_m. In other words, NLC measurement is compromised beyond these frequency limits. We performed stimulus frequency-dependent NLC measurements with this limitation in mind. NLC data obtained from cells with similar whole-cell parameters (R_s, R_m, and C_{lin}) were used for comparing the motor kinetics between wt-prestin vs. R130S-prestin. We found that NLC recorded from cells expressing R130S-prestin demonstrated a greater voltage stimulus-frequency dependence compared to wt-prestin expressing cells (Fig. 5). Although wt results are not statistically different, the NLC ratios plotted in Fig. 5c are reduced for R130S at

f_1=1562.5 and 3125 Hz. This result indicates that the R130S mutation slows the motor kinetics of prestin.

The aforementioned discrepancy between the amount of membrane-targeted R130S-prestin (~66% of wt-prestin, Fig. 3c) versus the magnitude of charge density of R130S-prestin (~33% of wt-prestin, Fig. 4d) can be at least partially explained by the slowed motor kinetics of R130S-prestin.

Effect of the R130S mutation on the anion transport function of prestin

Besides functioning as a voltage-operated motor, prestin also works as an anion transporter. Although its activity is weak [40], the overall prestin-derived anion transport activity could become significant since prestin is expressed in the OHC's lateral membrane at an extremely high level. Therefore, impairment of prestin's anion transport function could potentially compromise OHC function. In fact, prestin-KO mouse models show premature OHC loss [3, 5], and the cause of the cell death was speculated to be due to the lack of prestin-associated anion transport function [3].

In order to determine the effect of the R130S mutation on anion transport function, we performed an electrophysiological anion transport assay in the whole-cell configuration using thiocyanate (SCN^-), which is rapidly transported by SLC26 proteins and provides a large current signal. A previous study demonstrated that SCN^- is indeed transported by prestin [41]. This electrophysiological transport assay allows one to correct for observed anion transport activity by the amount of functional prestin in the cell membrane using NLC measurements from the same cells [41].

Figure 6a shows voltage-dependent whole-cell current responses of an R130S-prestin-expressing HEK293T cell before (black square), during (green circle), and after (grey triangle) extracellular perfusion of SCN^-. Whole-cell current at 0 mV holding potential was constantly measured throughout the experiment to monitor the perfusion and clearance of SCN^- (Fig. 6a, inset). The I–V curves shown in figure 6a were obtained at the time points indicated by arrows using the same color-code as in the inset. The difference in the currents indicates SCN^- transport. The magnitude of this SCN^--induced outward current at +120 mV was defined as Δcurrent, and plotted against C_{lin}, which correlates with cell size (Fig. 6b). We also recorded from untransfected HEK293T cells since endogenous transporters could mediate significant SCN^- transport. This was, in fact, the case since a positive correlation between Δcurrent vs. C_{lin} was found with statistical significance for untransfected cells ($r = 0.68$, $p = 0.015$, black diamonds in Fig. 6b). As expected, wt-prestin-expressing cells showed much greater current responses (blue circles in Fig. 6b) with statistically significant positive correlation ($r = 0.75$, $p < 0.0001$). R130S-prestin-expressing cells also showed large current responses (red triangles in Fig. 6b) with statistically significant positive correlation ($r = 0.61$, $p = 0.0008$). The F-test confirmed that the Δcurrent-C_{lin} relationships found in cells expressing wt-prestin and R130S-prestin were different from that found in untransfected cells ($p < 0.0001$ and $p = 0.0003$ for wt-prestin and R130S-prestin, respectively). These results indicate that R130S-prestin retains anion transport function. The F-test did not, however, find a difference in the Δcurrent-C_{lin} relationship between wt- vs. R130S-prestin-expressing cells ($p = 0.80$) despite the fact that R130S-prestin has membrane targeting issues

(Figs. 3), implying enhanced anion transport activity of R130S-prestin. In order to pursue this possibility, we replotted Δcurrent against Q_{max}, which correlates with the amount of prestin in the cell membrane (Fig. 6c). This exercise allowed us to find a greater positive correlation for both wt-prestin- ($r = 0.87$, $p < 0.0001$) and R130S-prestin-expressing cells ($r = 0.72$, $p < 0.0001$), reaffirming that the observed Δcurrents indeed associate with the anion transport activities of wt- and R130S-prestin. Difference in the anion transport activities between wt- vs. R130S-prestin became evident in this plot ($p < 0.0001$), suggesting that the R130S mutation does indeed augment prestin's anion transport activity. It should be noted that enhanced SCN^- transport activity does not necessarily indicate an increase in prestin's antiport activity for physiological substrates such as Cl^- and HCO_3^-. The result should be regarded as an indication of a potential adverse effect of the R130S mutation on the anion transport function of prestin, which may account for the disease phenotype.

As noted above, the slowed motor kinetics of R130S-prestin results in underestimation of the amount of functional prestin in the cell membrane. However, this would not affect the conclusion that the SCN^- transport function of R130S-prestin is enhanced compared to that of wt-prestin because the magnitudes of Δcurrent and the Δcurrent-C_{lin} relationships were similar between R130S- vs. wt-prestin (Fig. 6b) despite significant difference in their membrane targeting efficiencies (Fig. 3).

DISCUSSION

The premature translation termination caused by the W70X nonsense mutation likely induces nonsense-mediated mRNA decay [12]. Even if W70X-prestin were translated, it would not be targeted to the lateral membrane of OHCs since it does not contain any transmembrane domain. Therefore, it is probable that the W70X mutation manifests as a functional null, i.e., like a prestin knockout (prestin-KO) [3–6].

It is possible that both R130S- and W70X-prestin (if it is translated) can physically interact with wt-prestin in heterozygous individuals since prestin is known to form homooligomers [42–45]. It seems unlikely, however, that such potential physical interaction has any adverse effect on the function of wt-prestin since heterozygosity for these mutations does not induce hearing impairment [11]. Our previous study demonstrated functional independence of individual prestin molecules in an oligomeric complex [19], which is consistent with the recessive nature of human diseases associated with genetic mutations in SLC26 family members [1]. It is also known that normal cochlear operation can be attained with only one functional prestin allele. Previous studies reported autoregulation of prestin production in prestin-KO heterozygotes [46]. Another study demonstrated extremely high tolerance of cochlear function to drastically reduced prestin expression [47]. Hence, the normal hearing found in an individual heterozygous for the W70X mutation [11] should come as no surprise in light of these observations. These pieces of evidence could also account for normal hearing in an individual heterozygous for the R130S mutation [11], and also for why only a few variations in *SLC26A5* have been reported in association with hearing loss (OMIM 613865).

Significant functional alterations found in R130S-prestin – impaired membrane targeting, slowed motor kinetics, and enhanced SCN^- transport – appear to support a causal relationship of this mutation for the hearing loss found in young Japanese patients. Hearing impairment in one of the patients with compound heterozygous W70X/R130S mutations in prestin was reported to be quite severe [11], indicative of devastating hair cell damage and/or loss. Since prestin-KO mice are known to suffer premature OHC loss [3, 5], one possibility is that impaired membrane targeting of R130S-prestin and a possibly shortened dwell time in the membrane (even if this mutant is properly targeted to the cell membrane) result in prestin-KO-like consequences. A second possibility pertains to the impaired motor kinetics of R130S-prestin (Fig. 5). Premature OHC loss was unexpectedly observed in a mouse model expressing $prestin^{V499G/Y501H}$ [7]. This prestin mutant is targeted to the OHC lateral membrane, but has significantly depolarized V_{pk} and slowed motor kinetics [7, 19]. In other words, $prestin^{V499G/Y501H}$ is virtually a nonfunctional motor under physiological conditions. Although it remains elusive how these impaired motor characteristics of $prestin^{V499G/Y501H}$ link to premature OHC death, this observation serves as a precedent for the possibility that a change in motor kinetics is associated with hearing loss. In fact, the audiogram of one of the Japanese patients expressing mutated R130S prestin showed a much greater hearing impairment at high versus low stimulus frequencies such that the threshold at 250 Hz was 41 dB, while that at 4 kHz was 96 dB. Whether this frequency dependence reflects the reduced ability of R130S prestin to respond to voltage in a cycle-by-cycle manner remains to be determined. Modified anion transport activity of R130S-prestin could also have an adverse effect on OHC maintenance.

Significantly altered functional properties of R130S-prestin compared to its wild-type counterpart described in this study strongly suggest this missense mutation to be indeed pathogenic, and thus warrant future effort to generate R130S-prestin animal model to further investigate the mutation in its native environment, i.e., OHCs. Such an effort will provide opportunities to unequivocally confirm the pathogenicity of the prestin R130S mutation, and to distinguish the aforementioned possibilities in order to define the disease mechanism.

Acknowledgments

Nicole Chen (Stevenson High School, Lincolnshire, IL) contributed to the generation of the R130S prestin construct and the data collection at the early stage of this study. Imaging was performed at the Northwestern University Center for Advanced Microscopy, supported by NCI CCSG P30 CA060553 awarded to the Robert H Lurie Comprehensive Cancer Center. This work was supported by the National Institutes of Health grants [DC014553 to K.H., DC00089 to M.A.C., and DC011813 to J.Z.]; and the Hugh Knowles Hearing Center.

ABBREVIATIONS

OHC	outer hair cell
NLC	nonlinear capacitance
wt	wild-type
KO	knockout
ECFP	enhanced cyan fluorescent protein

References

1. Alper SL, Sharma AK. The SLC26 gene family of anion transporters and channels. Molecular Aspects of Medicine. 2013; 34:494–515. DOI: 10.1016/j.mam.2012.07.009 [PubMed: 23506885]
2. Zheng J, Shen W, He DZ, Long KB, Madison LD, Dallos P. Prestin is the motor protein of cochlear outer hair cells. Nature. 2000; 405:149–155. DOI: 10.1038/35012009 [PubMed: 10821263]
3. Liberman M, Gao J, He D, Wu X, Jia S, Zuo J. Prestin is required for electromotility of the outer hair cell and for the cochlear amplifier. Nature. 2002; 419:300–304. [PubMed: 12239568]
4. Cheatham MA, Huynh KH, Gao J, Zuo J, Dallos P. Cochlear function in Prestin knockout mice. J Physiol (Lond). 2004; 560:821–830. DOI: 10.1113/jphysiol.2004.069559 [PubMed: 15319415]
5. Wu X, Gao J, Guo Y, Zuo J. Hearing threshold elevation precedes hair-cell loss in prestin knockout mice. Brain Res Mol Brain Res. 2004; 126:30–37. DOI: 10.1016/j.molbrainres.2004.03.020 [PubMed: 15207913]
6. Cheatham MA, Zheng J, Huynh KH, Du GG, Edge RM, Anderson CT, Zuo J, Ryan AF, Dallos P. Evaluation of an independent prestin mouse model derived from the 129S1 strain. Audiol Neurootol. 2007; 12:378–390. DOI: 10.1159/000106481 [PubMed: 17664869]
7. Dallos P, Wu X, Cheatham MA, Gao J, Zheng J, Anderson CT, Jia S, Wang X, Cheng WHY, Sengupta S, et al. Prestin-Based Outer Hair Cell Motility Is Necessary for Mammalian Cochlear Amplification. Neuron. 2008; 58:333–339. DOI: 10.1016/j.neuron.2008.02.028 [PubMed: 18466744]
8. Liu XZ, Ouyang XM, Xia XJ, Zheng J, Pandya A, Li F, Du LL, Welch KO, Petit C, Smith RJ, et al. Prestin, a cochlear motor protein, is defective in non-syndromic hearing loss. Hum Mol Genet. 2003; 12:1155–1162. [PubMed: 12719379]
9. Tang HY, Xia A, Oghalai JS, Pereira FA, Alford RL. High frequency of the IVS2-2A>G DNA sequence variation in SLC26A5, encoding the cochlear motor protein prestin, precludes its involvement in hereditary hearing loss. BMC Med Genet. 2005; 6:30.doi: 10.1186/1471-2350-6-30 [PubMed: 16086836]
10. Shearer AE, Eppsteiner RW, Booth KT, Ephraim SS, Gurrola J 2nd, Simpson A, Black-Ziegelbein EA, Joshi S, Ravi H, Giuffre AC, et al. Utilizing ethnic-specific differences in minor allele frequency to recategorize reported pathogenic deafness variants. Am J Hum Genet. 2014; 95:445–453. DOI: 10.1016/j.ajhg.2014.09.001 [PubMed: 25262649]
11. Mutai H, Suzuki N, Shimizu A, Torii C, Namba K, Morimoto N, Kudoh J, Kaga K, Kosaki K, Matsunaga T. Diverse spectrum of rare deafness genes underlies early-childhood hearing loss in Japanese patients: a cross-sectional, multi-center next-generation sequencing study. Orphanet J Rare Dis. 2013; 8:172.doi: 10.1186/1750-1172-8-172 [PubMed: 24164807]
12. Fatscher T, Boehm V, Gehring NH. Mechanism, factors, and physiological role of nonsense-mediated mRNA decay. Cell Mol Life Sci. 2015; doi: 10.1007/s00018-00015-02017-00019
13. Gorbunov D, Sturlese M, Nies F, Kluge M, Bellanda M, Battistutta R, Oliver D. Molecular architecture and the structural basis for anion interaction in prestin and SLC26 transporters. Nat Commun. 2014; 5:3622.doi: 10.1038/ncomms4622 [PubMed: 24710176]
14. Kelley LA, Sternberg MJE. Protein structure prediction on the Web: a case study using the Phyre server. Nat Protoc. 2009; 4:363–371. DOI: 10.1038/nprot.2009.2 [PubMed: 19247286]
15. Geertsma ER, Chang Y-N, Shaik FR, Neldner Y, Pardon E, Steyaert J, Dutzler R. Structure of a prokaryotic fumarate transporter reveals the architecture of the SLC26 family. Nat Struct Mol Biol. 2015; 22:803–808. DOI: 10.1038/nsmb.3091 [PubMed: 26367249]
16. Homma K, Miller KK, Anderson CT, Sengupta S, Du GG, Aguiñaga S, Cheatham M, Dallos P, Zheng J. Interaction between CFTR and prestin (SLC26A5). Biochim Biophys Acta. 2010; 1798:1029–1040. S0005-2736(10)00041-6 [pii]. DOI: 10.1016/j.bbamem.2010.02.001 [PubMed: 20138822]
17. Crooks GE, Hon G, Chandonia J-M, Brenner SE. WebLogo: a sequence logo generator. Genome Res. 2004; 14:1188–1190. DOI: 10.1101/gr.849004 [PubMed: 15173120]
18. Santos-Sacchi J, Kakehata S, Takahashi S. Effects of membrane potential on the voltage dependence of motility-related charge in outer hair cells of the guinea-pig. J Physiol (Lond). 1998; 510(Pt 1):225–235. [PubMed: 9625879]

19. Homma K, Duan C, Zheng J, Cheatham MA, Dallos P. The V499G/Y501H mutation impairs fast motor kinetics of prestin and has significance for defining functional independence of individual prestin subunits. J Biol Chem. 2013; 288:2452–2463. DOI: 10.1074/jbc.M112.411579 [PubMed: 23212912]
20. Homma K, Dallos P. Evidence that prestin has at least two voltage-dependent steps. J Biol Chem. 2011; 286:2297–2307. DOI: 10.1074/jbc.M110.185694 [PubMed: 21071769]
21. Keller JP, Homma K, Duan C, Zheng J, Cheatham MA, Dallos P. Functional Regulation of the SLC26-Family Protein Prestin by Calcium/Calmodulin. J Neurosci. 2014; 34:1325–1332. DOI: 10.1523/JNEUROSCI.4020-13.2014 [PubMed: 24453323]
22. Pasqualetto E, Aiello R, Gesiot L, Bonetto G, Bellanda M, Battistutta R. Structure of the Cytosolic Portion of the Motor Protein Prestin and Functional Role of the STAS Domain in SLC26/SulP Anion Transporters. J Mol Biol. 2010; 400:448–462. DOI: 10.1016/j.jmb.2010.05.013 [PubMed: 20471983]
23. Pinedal T, Bonafè A, Superti-Furga A. Report of a novel mutation in the SLC26A2 gene found in a Colombian adult patient with diastrophic dysplasia. Rev Fac Med. 2013; 61:255–259.
24. Wedenoja S, Pekansaari E, Höglund P, Mäkelä S, Holmberg C, Kere J. Update on SLC26A3 mutations in congenital chloride diarrhea. Hum Mutat. 2011; 32:715–722. DOI: 10.1002/humu.21498 [PubMed: 21394828]
25. Chai Y, Huang Z, Tao Z, Li X, Li L, Li Y, Wu H, Yang T. Molecular etiology of hearing impairment associated with nonsyndromic enlarged vestibular aqueduct in East China. Am J Med Genet A. 2013; 161:2226–2233. DOI: 10.1002/ajmg.a.36068 [PubMed: 23918157]
26. López-Bigas N, Melchionda S, de Cid R, Grifa A, Zelante L, Govea N, Arbonés ML, Gasparini P, Estivill X. Identification of five new mutations of PDS/SLC26A4 in Mediterranean families with hearing impairment. Hum Mutat. 2001; 18:548.doi: 10.1002/humu.1238 [PubMed: 11748854]
27. Fugazzola L, Cerutti N, Mannavola D, Crino A, Cassio A, Gasparoni P, Vannucchi G, Beck-Peccoz P. Differential diagnosis between Pendred and pseudo-Pendred syndromes: clinical, radiologic, and molecular studies. Pediatr Res. 2002; 51:479–484. DOI: 10.1203/00006450-200204000-00013 [PubMed: 11919333]
28. Reyes S, Wang G, Ouyang X, Han B, Du LL, Yuan HJ, Yan D, Dai P, Liu XZ. Mutation analysis of SLC26A4 in mainland Chinese patients with enlarged vestibular aqueduct. Otolaryngol Head Neck Surg. 2009; 141:502–508. DOI: 10.1016/j.otohns.2009.07.004 [PubMed: 19786220]
29. Blons H, Feldmann D, Duval V, Messaz O, Denoyelle F, Loundon N, Sergout-Allaoui A, Houang M, Duriez F, Lacombe D, et al. Screening of SLC26A4 (PDS) gene in Pendred's syndrome: a large spectrum of mutations in France and phenotypic heterogeneity. Clin Genet. 2004; 66:333–340. DOI: 10.1111/j.1399-0004.2004.00296.x [PubMed: 15355436]
30. Van Hauwe P, Everett LA, Coucke P, Scott DA, Kraft ML, Ris-Stalpers C, Bolder C, Otten B, de Vijlder JJ, Dietrich NL, et al. Two frequent missense mutations in Pendred syndrome. Hum Mol Genet. 1998; 7:1099–1104. [PubMed: 9618166]
31. Anwar S, Riazuddin S, Ahmed ZM, Tasneem S, Ateeq-ul-Jaleel, Khan SY, Griffith AJ, Friedman TB, Riazuddin S. SLC26A4 mutation spectrum associated with DFNB4 deafness and Pendred's syndrome in Pakistanis. J Hum Genet. 2009; 54:266–270. DOI: 10.1038/jhg.2009.21 [PubMed: 19287372]
32. Pera A, Villamar M, Viñuela A, Gandía M, Medà C, Moreno F, Hernández-Chico C. A mutational analysis of the SLC26A4 gene in Spanish hearing-impaired families provides new insights into the genetic causes of Pendred syndrome and DFNB4 hearing loss. Eur J Hum Genet. 2008; 16:888–896. DOI: 10.1038/ejhg.2008.30 [PubMed: 18285825]
33. Chen K, Zong L, Liu M, Wang X, Zhou W, Zhan Y, Cao H, Dong C, Tang H, Jiang H. Developing regional genetic counseling for southern Chinese with nonsyndromic hearing impairment: a unique mutational spectrum. J Transl Med. 2014; 12:64.doi: 10.1186/1479-5876-12-64 [PubMed: 24612839]
34. Chen K, Wang X, Sun L, Jiang H. Screening of SLC26A4, FOXI1, KCNJ10, and GJB2 in bilateral deafness patients with inner ear malformation. Otolaryngol Head Neck Surg. 2012; 146:972–978. DOI: 10.1177/0194599812439670 [PubMed: 22412181]

35. Kumano S, Iida K, Ishihara K, Murakoshi M, Tsumoto K, Ikeda K, Kumagai I, Kobayashi T, Wada H. Salicylate-induced translocation of prestin having mutation in the GTSRH sequence to the plasma membrane. FEBS Lett. 2010; 584:2327–2332. DOI: 10.1016/j.febslet.2010.04.010 [PubMed: 20388516]
36. Ashmore JF. Forward and reverse transduction in the mammalian cochlea. Neurosci Res Suppl. 1990; 12:S39–50. [PubMed: 2243636]
37. Santos-Sacchi J. Reversible inhibition of voltage-dependent outer hair cell motility and capacitance. J Neurosci. 1991; 11:3096–3110. [PubMed: 1941076]
38. Albert JT, Winter H, Schaechinger TJ, Weber T, Wang X, He DZZ, Hendrich O, Geisler H-S, Zimmermann U, Oelmann K, et al. Voltage-sensitive prestin orthologue expressed in zebrafish hair cells. J Physiol (Lond). 2007; 580:451–461. DOI: 10.1113/jphysiol.2007.127993 [PubMed: 17272340]
39. Schaechinger TJ, Gorbunov D, Halaszovich CR, Moser T, Kügler S, Fakler B, Oliver D. A synthetic prestin reveals protein domains and molecular operation of outer hair cell piezoelectricity. Embo J. 2011; 30:2793–2804. DOI: 10.1038/emboj.2011.202 [PubMed: 21701557]
40. Mistrík P, Daudet N, Morandell K, Ashmore JF. Mammalian prestin is a weak Cl^-/HCO_3^- electrogenic antiporter. J Physiol (Lond). 2012; 590:5597–5610. DOI: 10.1113/jphysiol.2012.241448 [PubMed: 22890707]
41. Schänzler M, Fahlke C. Anion transport by the cochlear motor protein prestin. J Physiol (Lond). 2012; 590:259–272. DOI: 10.1113/jphysiol.2011.209577 [PubMed: 22063625]
42. Zheng J, Du G-G, Anderson CT, Keller JP, Orem A, Dallos P, Cheatham M. Analysis of the oligomeric structure of the motor protein prestin. J Biol Chem. 2006; 281:19916–19924. DOI: 10.1074/jbc.M513854200 [PubMed: 16682411]
43. Hallworth R, Nichols MG. Prestin in HEK cells is an obligate tetramer. J Neurophysiol. 2012; 107:5–11. DOI: 10.1152/jn.00728.2011 [PubMed: 21975444]
44. Mio K, Kubo Y, Ogura T, Yamamoto T, Arisaka F, Sato C. The motor protein prestin is a bullet-shaped molecule with inner cavities. J Biol Chem. 2008; 283:1137–1145. DOI: 10.1074/jbc.M702681200 [PubMed: 17998209]
45. Navaratnam D, Bai J, Samaranayake H, Santos-Sacchi J. N-terminal-mediated homomultimerization of prestin, the outer hair cell motor protein. Biophys J. 2005; 89:3345–3352. [PubMed: 16113116]
46. Cheatham MA, Zheng J, Huynh KH, Du GG, Gao J, Zuo J, Navarrete E, Dallos P. Cochlear function in mice with only one copy of the prestin gene. J Physiol (Lond). 2005; 569:229–241. DOI: 10.1113/jphysiol.2005.093518 [PubMed: 16166160]
47. Yamashita T, Fang J, Gao J, Yu Y, Lagarde MM, Zuo J. Normal hearing sensitivity at low-to-middle frequencies with 34% prestin-charge density. PLoS ONE. 2012; 7:e45453.doi: 10.1371/journal.pone.0045453 [PubMed: 23029017]
48. Mount DB, Romero MF. The SLC26 gene family of multifunctional anion exchangers. Pflugers Arch. 2004; 447:710–721. DOI: 10.1007/s00424-003-1090-3 [PubMed: 12759755]

Key messages

- Membrane targeting of prestin is impaired by the R130S missense mutation.
- The fast motor kinetics of prestin is impaired by the R130S missense mutation.
- Our study strongly suggests that the prestin R130S missense mutation is pathogenic.

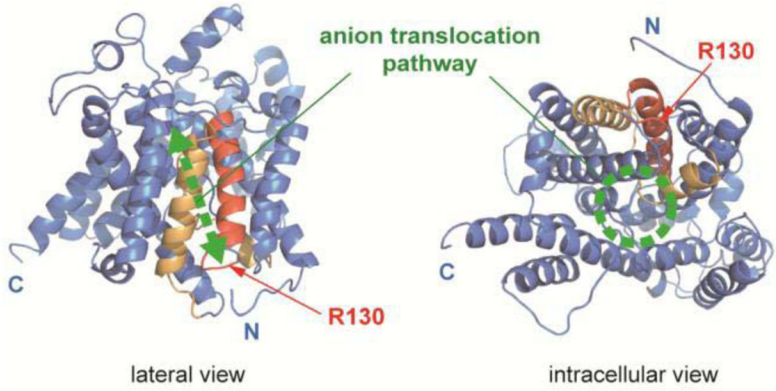

Fig. 1.

A prestin model. A structural model for the transmembrane region of prestin generated by Phyre2 is shown. The N- and C-terminal cytosolic domains are not shown in this model. The SulP and Saier motifs [13, 48] are highlighted in red and orange, respectively. Red arrows indicate the location of R130. A previously proposed anion translocation pathway [13] is also shown in green. “N” and “C” indicate the truncated N- and C-termini of the model.

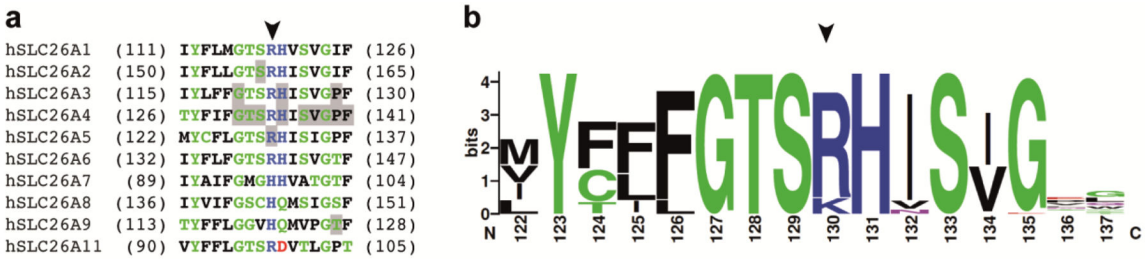

Fig. 2.

The R130 site and its vicinity. **a** Comparison of the amino acid sequence at the R130 site among the SLC26 gene family. A partial amino acid sequence (122–137) of human prestin (hSLC26A5) along with the corresponding sequences of other human SLC26 family members is shown. An arrowhead indicates the location of R130. Numbers in parentheses indicate the residue numbers at the beginning and the end of each segment. Locations of disease-associated missense mutations are highlighted in gray. Amino acids are colored according to their chemical properties: green for polar (G, S, T, Y, C, Q, and N), blue for basic (K, R, and H), red for acidic (D and E), and black for hydrophobic (A, V, L, I, P, W, F, and M) amino acids. **b** A graphical representation of amino acid residue conservation at the R130 site. The relative height of any given letter represents the frequency of that amino acid, while the total height of the stack represents the degree of sequence conservation (maximum 4.3 bits). Amino acids are colored in the same way as in (**a**). The numbers below the graphic indicate the residue numbers for human prestin. An arrowhead indicates the location of R130.

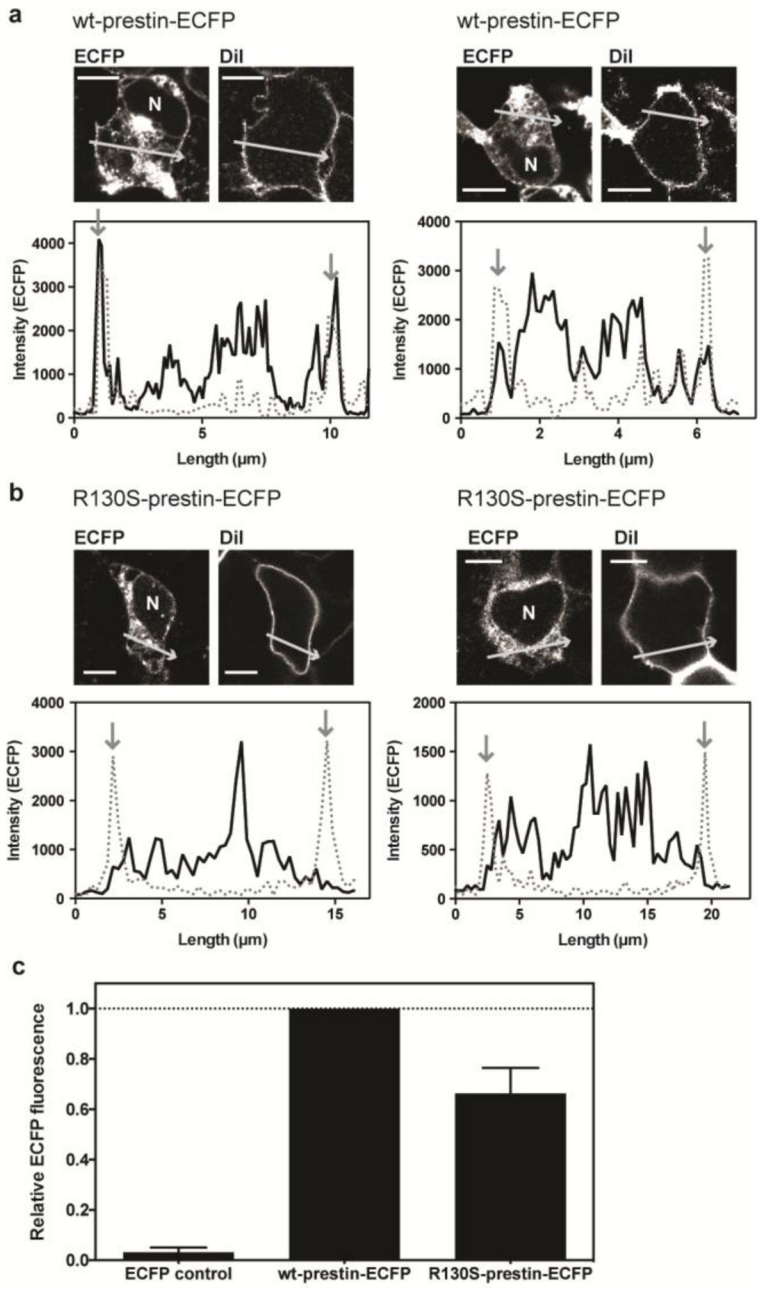

Fig. 3.

Subcellular localization of wild-type and R130S-prestin-ECFP in HEK293T cells. **a–b** Examples of HEK293T cells expressing wt-prestin-ECFP (**a**) and R130S-prestin-ECFP (**b**) are shown. The cells were stained with the plasma membrane marker, DiI. “N” indicates the nucleus. Scale bars (horizontal lines) indicate 5 and 10 μm for panels A and B, respectively. The plots below the images show ECFP fluorescence (solid lines) across the cell, as shown by the arrows in the companion images, along with the DiI fluorescence (broken lines). Vertical arrows indicate locations of the plasma membrane. **c** Quantification of membrane-targeted prestin. Wt- and R130S-prestin molecules targeted to the cell membrane were

biotinylated and isolated. The amounts of biotinylated prestin were determined by measuring ECFP fluorescence intensities (see the main text for details). ECFP intensities of control (ECFP alone, left column) and R130S-prestin-ECFP (right column) were 3 ± 2% (n=2) and 66 ± 10% (n=4), respectively, compared to wt-prestin-CFP (normalized to 100% for each experimental repeat, n=4), and these differences were statistically significant (p-values were 0.0056 and 0.0069, respectively). The error bars indicate standard deviations.

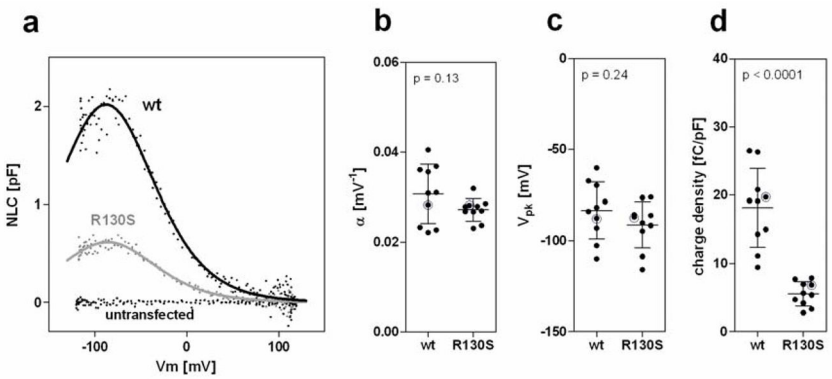

Fig. 4.

Functional consequences of the R130S mutation on motor function. **a** Representative Cm recordings are shown from a wt-prestin-ECFP-expressing cell and an R130S-prestin-ECFP-expressing cell along with that from an untransfected cell. **b–d** The α, V_{pk}, and charge density (defined as Q_{max}/C_{lin}) values were as follows: wt-prestin [0.031 ± 0.007 mV^{-1}, −83 ± 16 mV, 18 ± 6 fC/pF (n=10)]; R130S-prestin [0.027 ± 0.002 mV^{-1}, −91 ± 13 mV, 6 ± 2 fC/pF (n=10)]. The horizontal solid lines indicate the means and standard deviations. The NLC data shown in panel **a** are highlighted in gray in panels **b**, **c**, and **d**.

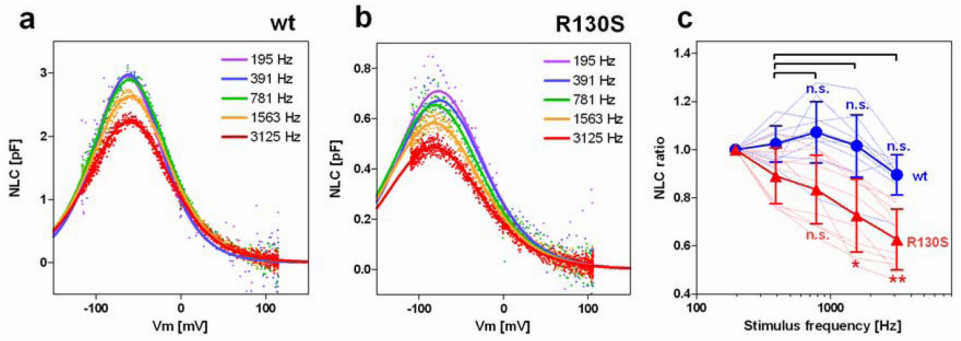

Fig. 5.

Functional effect of the R130S mutation on motor kinetics. NLC was measured using five different f_1 frequencies (195, 390, 781, 1563, and 3125 Hz) with the corresponding f_2 frequencies being twice as large as f_1. Representative recordings for wt-prestin-ECFP (**a**) and R130S-prestin-ECFP (**b**) are shown. The obtained Q_{max} values were divided by those determined at 195 Hz, and resulting quotients plotted against the f_1 stimulus frequency in panel **c**. The results for wt-prestin (n=10) and R130S-prestin (n=10) are shown in blue and red, respectively as means and standard deviations. Thin broken lines indicate individual recordings whereas the thick solid lines indicate the means. Single and double asterisks indicate statistical significance with $p<0.05$ and $p<0.01$, respectively. “n.s.” indicates $p>0.05$. The p-values were computed using a Tukey multiple comparison test.

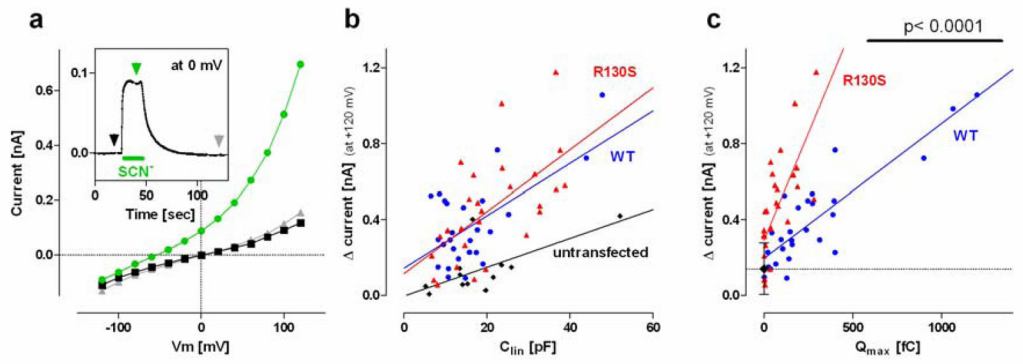

Fig. 6.

Functional consequence of R130S on anion transport. **a** Thiocyanate (SCN^-) was extracellularly applied to an R130S-prestin-ECFP-expressing HEK293T cell during the time period indicated by the green bar shown in the inset. Membrane conductance was constantly measured throughout the experiment to monitor the effect of SCN^- (inset). IV relations were determined at three different time points indicated by arrowheads in the inset with the same color-code as the IV curves. The magnitude of SCN^--induced outward current at +120 mV is defined as 'Δcurrent'. **b** Plots of Δcurrent against the linear membrane capacitance of the cell, C_{lin}. **c** Plots of Δcurrent versus Q_{max}. A black diamond with error bars (s.d.) and the broken horizontal line indicate the mean value of the results obtained from untransfected cells in panel **b**. The number of recordings were 12, 27, and 27 for the untransfected control, wt-prestin, and R130S-prestin, respectively.